

## Facile total synthesis of lysicamine and the anticancer activities of the Ru<sup>II</sup>, Rh<sup>III</sup>, Mn<sup>II</sup> and Zn<sup>II</sup> complexes of lysicamine

Jiao-Lan Qin<sup>1,\*</sup>, Ting Meng<sup>1,\*</sup>, Zhen-Feng Chen<sup>1</sup>, Xiao-Li Xie<sup>1</sup>, Qi-Pin Qin<sup>1</sup>, Xiao-Ju He<sup>1</sup>, Ke-Bin Huang<sup>1</sup> and Hong Liang<sup>1</sup>

<sup>1</sup>State Key Laboratory for Chemistry and Molecular Engineering of Medicinal Resources, School of Chemistry and Pharmacy, Guangxi Normal University, Guilin 541004, P. R. China

\*These authors have contributed equally to this work

Correspondence to: Hong Liang, email: hliang@gxnu.edu.cn

Zhen-Feng Chen, email: chenzf@gxnu.edu.cn

Keywords: lysicamine, metal complexes, antitumor activity, apoptosis

Received: May 09, 2017

Accepted: June 19, 2017

Published: July 26, 2017

Copyright: Qin et al. This is an open-access article distributed under the terms of the Creative Commons Attribution License 3.0 (CC BY 3.0), which permits unrestricted use, distribution, and reproduction in any medium, provided the original author and source are credited.

### ABSTRACT

Lysicamine is a natural oxoaporphine alkaloid, which isolated from traditional Chinese medicine (TCM) herbs and has been shown to possess cytotoxicity to hepatocarcinoma cell lines. Reports on its antitumor activity are scarce because lysicamine occurs in plants at a low content. In this work, we demonstrate a facile concise total synthesis of lysicamine from simple raw materials under mild reaction conditions, and the preparation of the Ru(II), Rh(III), Mn(II) and Zn(II) complexes 1–4 of lysicamine (LY). All the compounds were fully characterized by elemental analysis, IR, ESI-MS, <sup>1</sup>H and <sup>13</sup>C NMR, as well as single-crystal X-ray diffraction analysis. Compared with the free ligand LY, complexes 2 and 3 exhibited superior *in vitro* cytotoxicity against HepG2 and NCI-H460. Mechanistic studies indicated that 2 and 3 blocked the cell cycle in the S phase by decreasing of cyclins A2/B1/D1/E1, CDK 2/6, and PCNA levels and increasing levels of p21, p27, p53 and CDC25A proteins. In addition, 2 and 3 induced cell apoptosis via both the caspase-dependent mitochondrial pathway and the death receptor pathway. *in vivo* study showed that 2 inhibited HepG2 tumor growth at 1/3 maximum tolerated dose (MTD) and had a better safety profile than cisplatin.

### INTRODUCTION

Many oxoaporphine alkaloids are derived from traditional Chinese medicine (TCM) herbs and exhibit various pharmacological properties, such as antiplatelet aggregation [1], anti-inflammation [2], antitubercular [3] and antitumor activities [4, 5], *etc.* These medicinally interesting compounds generally have very low content (<0.01%) in plants, and their biological activities are thus reported only scarcely.

Some research teams have devoted considerable efforts to synthesize oxoaporphine alkaloids [6-9]. Oxidation of aporphines is the easiest way to produce oxoaporphines, and this has allowed the synthesis of

glaucine [10], diisopropylboldine [11], and (+)-boldine [12, 13]. However, the source aporphines have limited commercial supply. The total synthesis of oxoaporphines has been reported both in the early years [6-9] and recently [14-16]. The reported syntheses have clear disadvantages, including numerous reaction steps, long reaction time, harsh reaction conditions, complicated work-up procedures, extensive use of organic solvents, *etc.* Needless to say, a short and efficient route for the total synthesis of oxoaporphine alkaloids is urgently needed.

Because of the side effects of cisplatin in chemotherapy, non-platinum metal-based antitumor agents that are highly efficient and less toxic are sought after in recent decades [17, 18]. Among thousands of

candidates, three ruthenium complexes, *i.e.*, [ImH] [*trans*-RuCl<sub>4</sub>(DMSO)Im] (NAMI-A) [19], [ImH] [*trans*-RuCl<sub>4</sub>Im<sub>2</sub>] (KP1019) [20], and Na[*trans*-RuCl<sub>4</sub>Im<sub>2</sub>] (NKP-1339 or IT-139) [21] are currently tested in clinical trials as anticancer drugs. Besides, the complexes of Rh(III) [22-26], Zn(II) [27-29], and Mn(II) [30, 31] with potential antitumor activity have also been reported.

An increasing number of studies indicate that coordination compounds based on traditional Chinese medicines (TCMs) have excellent antitumor activity [32]. We previously reported on the antitumor activity of liriodenine, oxoglucine, and oxoisoaporphine, and demonstrated that the efficacy was much higher in the liriodenine metal complexes (with Pt<sup>II</sup>, Ru<sup>II</sup>, Mn<sup>II</sup>, Fe<sup>II</sup>, Co<sup>II</sup>, and Zn<sup>II</sup>) [33, 34], oxoglucine metal complexes (with Au<sup>III</sup>, Zn<sup>II</sup>, Co<sup>II</sup>, Mn<sup>II</sup>, Y<sup>III</sup>, and Dy<sup>III</sup>) [12, 13], and oxoisoaporphine metal complexes (with Ni<sup>II</sup>, Pd<sup>II</sup> and Pt<sup>II</sup>) [35, 36] compared with that of the corresponding ligands.

Primary screening results revealed that lysicamine had cytotoxicity against hepatocarcinoma cell lines [37] and human adult T-cell leukemia/lymphoma (III) [38]. In this study, we demonstrate a very efficient route to synthesize lysicamine from simple starting materials under mild conditions. In addition, four metal complexes of lysicamine, *i.e.*, [Ru(LY)Cl<sub>2</sub>(DMSO)<sub>2</sub>] $\cdot$ 3H<sub>2</sub>O (**1**), [Rh(LY-OH)Cl<sub>3</sub>CH<sub>3</sub>OH] (**2**), [Mn(LY)<sub>3</sub>(ClO<sub>4</sub>)<sub>2</sub>] $\cdot$ 3CHCl<sub>3</sub> (**3**), and [Zn(LY)<sub>2</sub>(ClO<sub>4</sub>)<sub>2</sub>] (**4**), were synthesized and fully characterized. The cytotoxicity and antitumor mechanism of these metal complexes were investigated. The *in vivo* antitumor efficacy of **2** was further evaluated in HepG2 xenograft nude mice models.

## RESULTS

### Total synthesis of lysicamine (LY)

Figure 1 shows the synthetic route, which started with commercially available starting materials, 2-bromophenylacetic acid and 3,4-dimethoxyphenethylamine. The amide (**1**) was obtained from amide coupling reaction. Specifically, 2-bromophenylacetic acid was treated with SOCl<sub>2</sub> in CHCl<sub>3</sub> to generate 2-bromophenylacetyl chloride, which in turn reacted with 3,4-dimethoxyphenethylamine in CHCl<sub>3</sub> to give amide (**1**) as white needles in 85% yield. The Bischler–Napieralski reaction [39] was employed for the cyclization of (**1**) and furnish the tetrahydroisoquinolines (**II**). The intermediate imine was reduced by (CH<sub>3</sub>COO)<sub>3</sub>BHNa without further purification [40] to afford (**II**) in 82% yield.

Previously reports [41-43] often constructed the ring C of the aporphine nucleus through radical-initiated cyclization. However, direct radical cyclization of (**II**) was unsuccessful, probably because there was no substituent on the N atom of the tetrahydroisoquinoline [44]. If tetrahydroisoquinoline could carry a bulky substituent on the N atom, such as a COOEt group, the corresponding aporphine could be prepared in good

yield. Therefore, we ran the acylation of (**II**) with one equivalent ClCOOCH<sub>3</sub> in CHCl<sub>3</sub> on ice-bath for 1h to obtain the tetrahydroisoquinoline (**III**) in 88% yield. Radical cyclization of (**III**) using tricyclohexyl phosphine and Pd(OAc)<sub>2</sub> in dry DMA at 135 °C under N<sub>2</sub> protection for 5 h then gave intermediate (**IV**) in 84% yield [45]. Afterwards, (**IV**) was deprotected with LiAlH<sub>4</sub> in anhydrous THF to give nuciferine (**V**) in 56% yield [45].

Previous reports showed that compared with other oxidants including PhI(OAc)<sub>2</sub>, lead(IV) acetate, HIO<sub>4</sub>, and iodobenzene diacetate (IBD), manganese(III) acetate was less toxic and could give good yield and less by-products [11]. Therefore, manganese(III) acetate was chosen as the oxidizing agent to transform compound (**V**) to lysicamine (LY). The oxidation reaction proceeded in glacial acetic acid at 80 °C for 12 h. Further purification by silica gel chromatography (CH<sub>2</sub>Cl<sub>2</sub>/MeOH/NH<sub>3</sub>(aq) = 98:1:1) retrieved more lysicamine (LY) as yellow needles in 23% yield.

Note that although the final oxidation had very poor yield, the synthesis of compounds (**I**)–(**V**) did not require purification by silica gel chromatography. Instead, crude materials were always used in the next step, and good yields were still obtained (82%–88%, 56% for (**V**)). The overall synthesis required only six steps, whereas the latest report that used Fremy's salt as an effective oxidizing agent required nine steps to prepare the lysicamine end product [16]. Our route is clearly beneficial to the synthesis of a large number of lysicamine and related oxoaporphine alkaloids. We also alleviated the consumption of large amounts of organic solvents that were required in other reports for purification [14, 15].

### Synthesis and structural characterization of 1–4

The metal complexes [Ru(LY)Cl<sub>2</sub>(DMSO)<sub>2</sub>] $\cdot$ 3H<sub>2</sub>O(**1**), [Rh(LY-OH)Cl<sub>3</sub>CH<sub>3</sub>OH] (**2**), [Mn(LY)<sub>3</sub>(ClO<sub>4</sub>)<sub>2</sub>] $\cdot$ 3CHCl<sub>3</sub> (**3**), and [Zn(LY)<sub>2</sub>(ClO<sub>4</sub>)<sub>2</sub>] (**4**) were synthesized by reaction of LY with cis-RuCl<sub>2</sub>(DMSO)<sub>4</sub>, RhCl<sub>3</sub> $\cdot$ H<sub>2</sub>O, Zn(ClO<sub>4</sub>)<sub>2</sub> $\cdot$ 6H<sub>2</sub>O, and Mn(ClO<sub>4</sub>)<sub>2</sub> $\cdot$ 6H<sub>2</sub>O in 2:1 MeOH/CHCl<sub>3</sub>, respectively. The metal complexes were characterized by IR, ESI-MS and elemental analyses (<sup>1</sup>H NMR and <sup>13</sup>C NMR were used for **2**). Their crystal structures were determined by single-crystal X-ray diffraction analysis.

### Crystal structures

Supplementary Tables 1 and 3 summarize the crystal data and refinement details of **I**, **III**, **IV**, LY and of **1**–**4**, respectively. Supplementary Tables 2 and 4 list the selected bond lengths and angles of the corresponding compounds. Figure 2 shows the crystal structures of **1**–**4** (see Supplementary Figure 1 for the crystal structures of **I**, **III**, **IV** and LY). The complexes **1**–**4** had mononuclear structures and the central metal ion adopted the six-coordinated distort geometry. The Ru<sup>II</sup> or Rh<sup>III</sup> ions of **1**

and **2** were coordinated by N and O from one LY ligand, two Cl and two DMSO via the S atom (for **1**), three Cl and one methanol (for **2**), to form a distorted octahedral geometry. It is worth noting that in complex **2**, one  $-OCH_3$  group of LY changed to  $-OH$ . In **3** and **4**, the  $Mn^{II}$  centre ion was coordinated by N and O from three LY ligands, and the  $Zn^{II}$  ion was associated with the N and O atoms from two LY ligands and the O atom from two  $ClO_4^-$ .

To determine the stability of the metal complexes, the TBS solutions (Tris-KCl buffer solution with pH value of 7.35, containing 1% DMSO) of **1–4** were prepared and the UV-Vis spectra were recorded at 0 h, 2 h, 4 h, 8 h,

12 h and 24 h (Supplementary Figure 2). Complexes **2** and **3** were also examined on HPLC (Supplementary Figure 3). No obvious changes were observed in the UV-Vis spectra and HPLC chromatograms. Hence, **1–4** were stable in TBS and DMSO at room temperature for 24 h.

### Inhibition of the proliferation of human cancer cells

The inhibitory effects of LY, **1–4** and the corresponding metal salts were tested against BEL-7404, HepG2, NCI-H460, and T-24 cancer cells and the normal

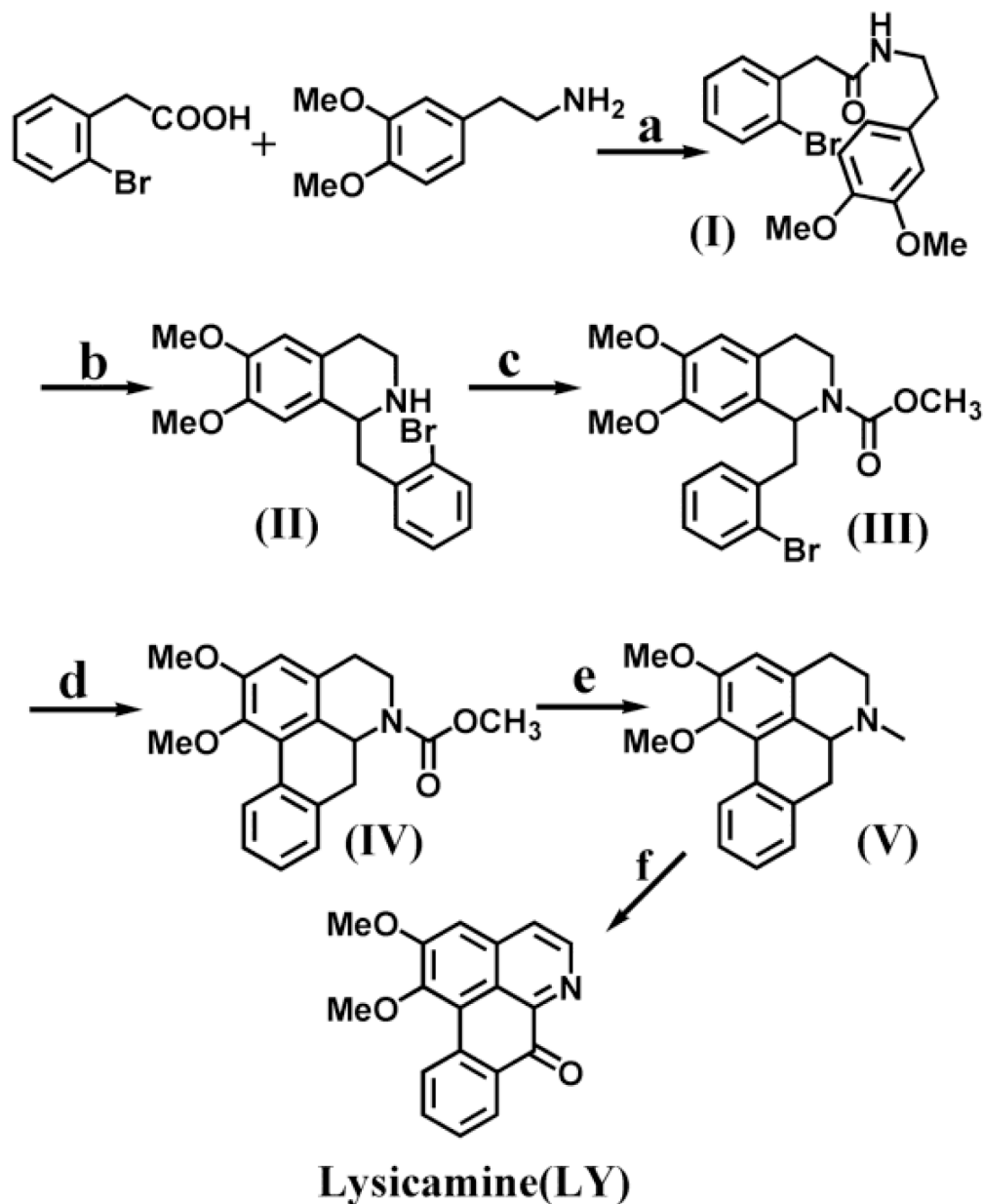


**Figure 1: Synthetic routes of lysicamine (LY).** Reagents and conditions are as follows: a: (i)  $SOCl_2$ ,  $CHCl_3$  (75 °C reflux, 2 h); (ii)  $CHCl_3$ ,  $NaHCO_3$  (ice-bath, 2 h); b: (i)  $POCl_3$ , toluene (80 °C reflux, 3 h); (ii)  $(CH_3COO)_3BHN$ ,  $CHCl_3$  (room temperature, 1 h); c: Methyl chloroformate ( $ClCOOCH_3$ ),  $NaOH$ ,  $CHCl_3$  (room temperature, 1 h); d: tricyclohexyl phosphine [ $P(cy)_3$ ],  $Pd(OAc)_2$ ,  $K_2CO_3$ , DMA (120 °C,  $N_2$ , 5 h); e:  $LiAlH_4$ , THF (reflux, 6 h); f:  $Mn(Ac)_3$ , glacial acetic acid (80 °C, 12 h).

**Table 1: The <sup>a</sup>IC<sub>50</sub> values (μM) of LY, 1–4 and cisplatin for the four tumour cells and the HL-7702 normal liver cell**

Compound	BEL-7404	HepG2	NCI-H460	T-24	HL-7702
LY	47.52±1.65	23.90±0.41	19.14±0.18	34.50±1.96	29.27±0.72
<b>1</b>	49.52±0.53	57.31±3.32	15.76±2.31	20.68±1.83	69.21±1.81
<b>2</b>	18.37±0.14	7.56±2.91	10.01±2.39	14.29±1.05	35.08±3.34
<b>3</b>	36.24±1.03	14.51±0.69	12.89±3.62	15.42±1.81	55.36±3.65
<b>4</b>	29.67±0.96	35.46±3.99	8.17±1.69	16.25±0.93	34.59±2.21
<sup>b</sup> Cisplatin	12.41±0.38	18.51±0.78	18.29±1.02	28.07±1.88	15.67±1.27

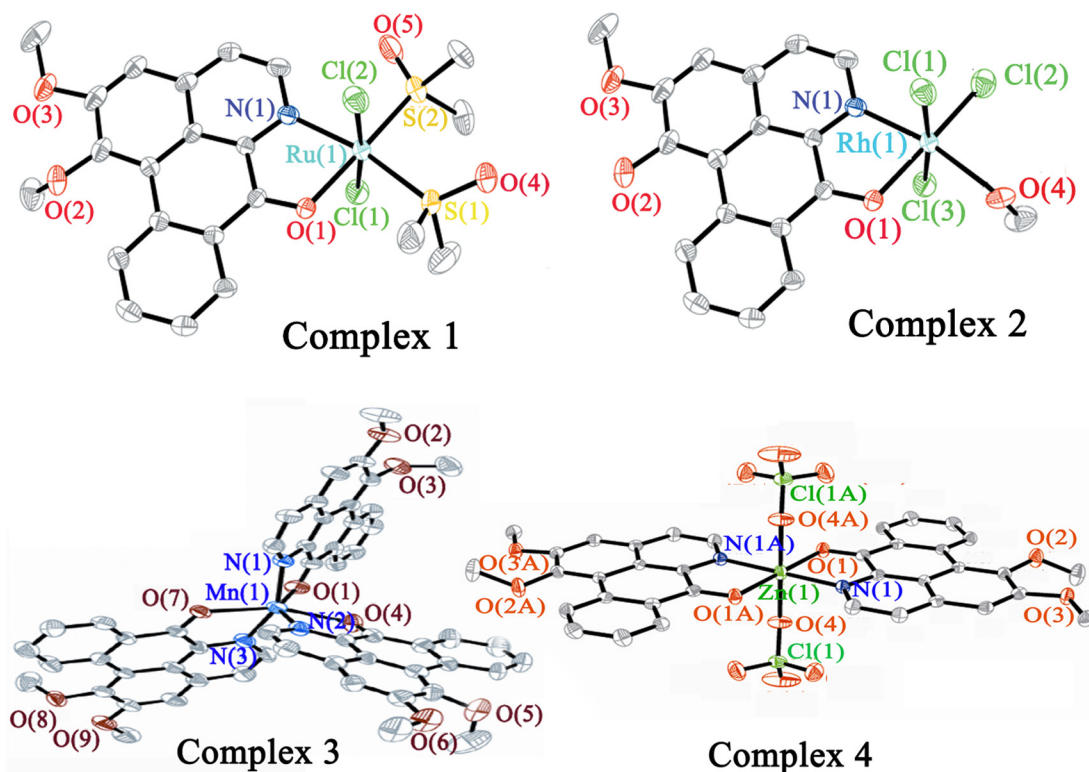
<sup>a</sup>IC<sub>50</sub> values are presented as the mean ± SD from five independent experiments. <sup>b</sup>Cisplatin was dissolved at a concentration of 1mM in 0.154 M NaCl [46].

liver cell HL-7702 in the MTT assay with cisplatin as the positive control. All cells were incubated with compounds at 20 μM for 48 h. Supplementary Table 5 shows that the inhibitory rates of LY and **1–4** varied in 31%–74% against the selected tumor cells, except for **1** and **4** gave 18.83% and 20.39% inhibition against HepG2 cells, respectively. Remarkably, **2** and **3** were highly cytotoxic against HepG2 cells (74.90% and 62.99%) and against NCI-H460 (63.82% and 54.93%). Besides, **2** and **3** were less toxic to normal liver cell HL-7702 (15.1% and 32.9%) than LY(45.5%) and cisplatin (68.9%). Thus, **2** and **3** may be potential safe candidates as an anticancer agent. Table 1 shows that **2** and **3** had much lower IC<sub>50</sub> values

(7–15 μM) than LY and cisplatin against all selected tumor cell lines except BEL-7404. Among them, HepG2 cells showed the highest sensitivity to **2** and **3** with IC<sub>50</sub> value of 7.56±2.91 and 14.51±0.69 μM, which were approximately 1.6–3.2 fold increased comparing with the free LY ligand. Therefore, the HepG2 cells were selected for studying the antitumor mechanism of **2** and **3**.

#### Uptake of metal complexes in HepG2 cells

The cellular uptake and distribution of the complexes would help to elucidate the target site and pathways [47, 48]. The distribution of the metal (Rh and Mn) in the two

**Figure 2: Crystal structures of complexes 1–4.**

cellular fractions of the HepG2 cells was investigated by ICP-MS according to the reported method [49] (see in Supplementary Figure 4). The results showed that after exposing the HepG2 cells to **2** (7.0  $\mu\text{M}$ ) or **3** (14.0  $\mu\text{M}$ ) for 8 h, the amount of Rh or Mn was higher in the mitochondrial fraction than in the nuclear fraction. Therefore, the mitochondria were a potential target site for **2** and **3**.

### Cell cycle distribution

The effects of **2** and **3** on the cell cycle progression of HepG2 cells were determined by flow cytometry (Figure 3A). Complexes **2** and **3** caused significant cell cycle arrest at the S phase in a dose-dependent manner after incubation for 24 h. In the presence of **2** at 3.5, 7.0, and 14.0  $\mu\text{M}$ , the population of the HepG2 cells in the S phase increased from 31.23% to 55.23%, 79.34% and 80.80%, respectively. Similarly, the population of HepG2 cells in the S phase increased from 31.23% to 48.70% when 28.0  $\mu\text{M}$  **3** was applied. The findings were consistent with the results of the *in vitro* cytotoxicity and also indicated that **2** was more active than **3** towards HepG2 cells. In contrast,  $\text{Mn}(\text{ClO}_4)_2 \cdot 6\text{H}_2\text{O}$  (16.0  $\mu\text{M}$ ) and  $\text{RhCl}_3 \cdot 3\text{H}_2\text{O}$  (16.0  $\mu\text{M}$ ) did not significantly induce the cell cycle arrest. In brief, we assumed that the antiproliferative effects of **2** and **3** resulted mainly from inducing cell cycle arrest in the S phase. Since LY only blocked the cell cycle in the G1 phase, the cytotoxicity of **2** and **3** must come from different mechanisms. The unique activities of **2** and **3** must be ascribed to the Rh(III) and Mn(II) center in the complexes.

### Expression of proteins related to cell cycle

HepG2 cells were incubated with **2** and **3** at increasing concentrations for 24 h, and the expression of cell cycle regulatory proteins in the S phase was examined through Western blot analysis. Figure 3B–3E and Supplementary Figure 5 shown that **2** and **3** decreased the expression of cyclin A2, cyclin B1, cyclin D1, cyclin E1, Cdc25A, p-Cdk2, and Cdk6 in a concentration-dependent manner. In contrast, **2** and **3** increased the expression of Cdk2, p-Cdc25A, p53, p21 and p27, also in a concentration-dependent manner. It could thus be concluded that **2** and **3** induced S phase arrest in the cell cycle by activating the p53, p21 and p27 proteins and inhibiting cyclin A2/CDK2, cyclin D1/CDK2,6, and cyclin E1/CDK2 [50–52]. Furthermore, **2** and **3** also decreased the proliferating cell nuclear antigen (PCNA) level, which is a key factor in DNA replication and cell cycle regulation [53], indicating that DNA synthesis was inhibited and the cell cycle was arrested in the S phase [54].

### Cell apoptosis

The Hoechst33258 assay is commonly used to measure the changes in cell morphology caused by

apoptosis [55]. The HepG2 cells were incubated with **2** (3.5, 7.0, and 14.0  $\mu\text{M}$ ) and **3** (7.0, 14.0, and 28.0  $\mu\text{M}$ ) for 24 h, respectively, then stained with Hoechst33258 and examined under a fluorescence microscope (Figure 4A). Compared with control HepG2 cells, these cells treated with **2** and **3** gave stronger fluorescence in a dose-dependent manner, and the changes in cell morphology included irregular nuclei, chromatin shrinkage, and formation of apoptotic bodies, all of which indicated cell apoptosis.

To further examine the apoptosis of HepG2 cells triggered by **2** and **3**, the cells were incubated with **2** and **3** for 24 h, then stained with both Annexin V-FITC and PI before analysis by flow cytometry [56]. Figure 4B shows that treatment with **2** (3.5, 7.0, and 14.0  $\mu\text{M}$ ) and **3** (7.0, 14.0 and 28.0  $\mu\text{M}$ ) significantly increased the percentage of apoptotic cells (Q2 and Q3). After treating the HepG2 cells with 14.0  $\mu\text{M}$  **2** (respectively 28.0  $\mu\text{M}$  **3**), the percentages of cells undergoing apoptosis and necrosis increased from 4.1% to 41.2% (respectively to 35.8%).

### Expression of apoptosis-related proteins

To further confirm that **2** and **3** induced apoptosis in HepG2 cells, Western blot analysis was used to examine the protein expression of C-myc, Bcl-2, Bcl-xl, Bax, Apaf-1 and cytochrome *c* (Figure 4C–4F).

After the HepG2 cells were incubated with **2** and **3** for 24 h at various concentrations, the expression of C-myc, Bcl-xl and Bcl-2 decreased, and the expression of Bax, Apaf-1 and cytochrome *c* increased. The degree of increase (or decrease) depended on the concentration of **2** and **3**. It could be concluded that the increase in pro-apoptotic factor (Bax) formed the mitochondrial apoptosis-induced channel (MAC), which mediated the release of cytochrome *c* from mitochondria to the cytosol, and promoted the activation of caspase-9/-3, ultimately leading to cell apoptosis [57].

### The level of reactive oxygen species (ROS), intracellular $\text{Ca}^{2+}$ , and mitochondria membrane potential ( $\Delta\Psi\text{m}$ ) in HepG2 cells

The cell uptake assay showed that the amount of Rh and Mn was higher in the mitochondria than in the nuclear fraction, and indicated that **2** and **3** probably targeted the mitochondria to cause cell apoptosis. The overproduction of ROS [58, 59], increase of intracellular  $\text{Ca}^{2+}$  [60], and loss of mitochondrial membrane potential (MMP,  $\Delta\Psi\text{m}$ ) [61] can all lead to mitochondrial dysfunction, and they thus play a central role in apoptosis [62].

The effects of **2** and **3** on the ROS, intracellular  $\text{Ca}^{2+}$  and  $\Delta\Psi\text{m}$  of HepG2 cells are shown in Figure 5 and Supplementary Figure 6. The changes in the ROS level, intracellular  $\text{Ca}^{2+}$  and loss of  $\Delta\Psi\text{m}$  in the HepG2 cells were detected by the DCFH-DA, Fluo-3 AM, and

JC-1 fluorescent probes, respectively (see in Figure 5A). Green fluorescence represented higher ROS levels, more intracellular  $Ca^{2+}$ , and reduced  $\Delta\Psi_m$ . In the control cells, little green fluorescence was observed, suggesting

that the levels of ROS and  $Ca^{2+}$  were very low. The cells exposed to **2** (3.5, 7.0 and 14.0  $\mu\text{M}$ ) for 24 h gave green fluorescence with escalating intensity in a dose-dependent manner, which indicated the increase of ROS

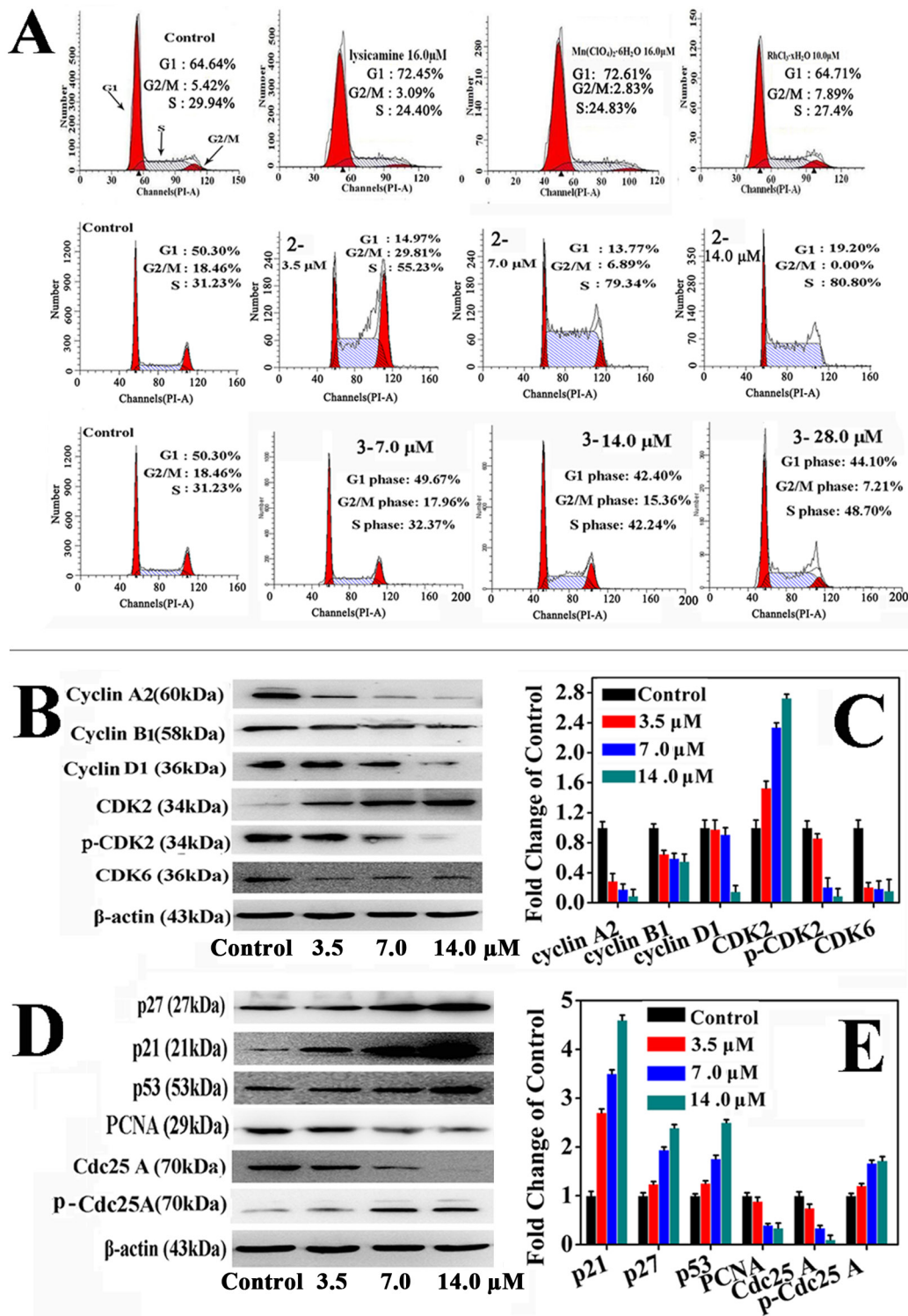


**Figure 3: The effects of **2** and **3** treatment in HepG2 cells on cell cycle. (A) Cell cycle analysis of **2**, **3**, LY and metal salt in HepG2 cells. (B, D) Effects of **2** treatment in HepG2 cells on cell cycle regulatory proteins at 3.5, 7.0 and 14.0  $\mu\text{M}$  for 24 h, respectively. (C, E) The relative protein expression of each band = (density of each band/density of  $\beta$ -Actin band). Mean  $\pm$  SD was from three independent measurements.**

and  $\text{Ca}^{2+}$ , as well as the loss of  $\Delta\Psi_m$ . As a confirmation, flow cytometry analysis (Figure 5B) also showed that **2** greatly increased the ROS and  $\text{Ca}^{2+}$  levels and promoted

the loss of  $\Delta\Psi_m$  in the HepG2 cells (blue, orange, and green lines). Compared with the control cells (red line), the treated cells differed notably in the intracellular

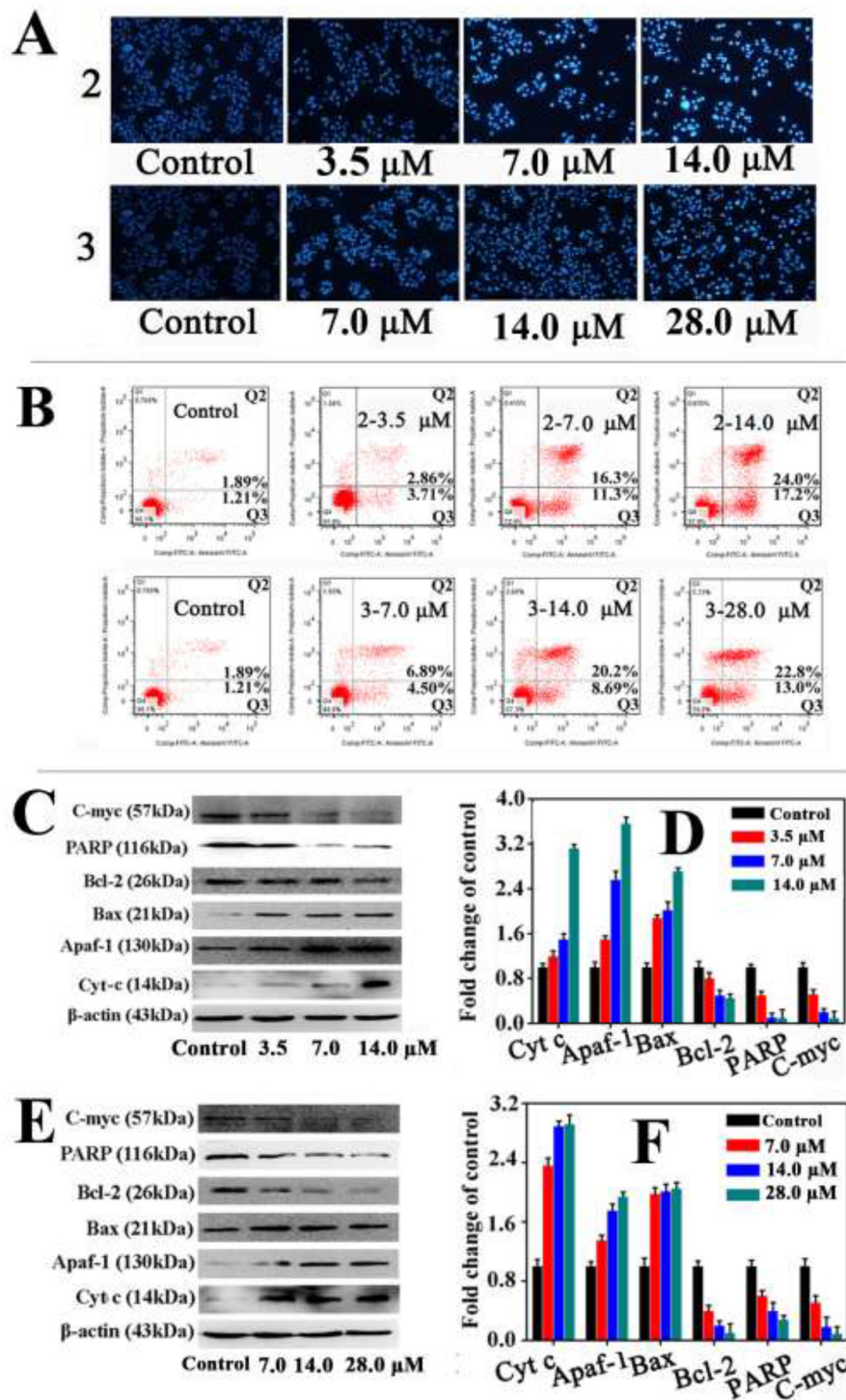


**Figure 4: Apoptosis of HepG2 cells induced by 2 and 3.** (A) The apoptotic nuclear morphological analysis by Hoechst-33258 staining(magnification 100 $\times$ ) and (B) the apoptosis of HepG2 cells analysis by flow cytometry after 24 h treatment with **2** and **3** at variously concentrations for 24 h. (C, E) Western blot analysis of apoptosis associated proteins after treatment of HepG2 cells with **2** (3.5, 7.0 and 14.0  $\mu\text{M}$ ) and **3** (7.0, 14.0 and 28.0  $\mu\text{M}$ ) for 24 h, respectively. (D, F) Densitometry analysis from part C and E. The relative expression of each band = (density of each band/density of  $\beta$ -actin band). Mean and SD values were from three independent measurements.

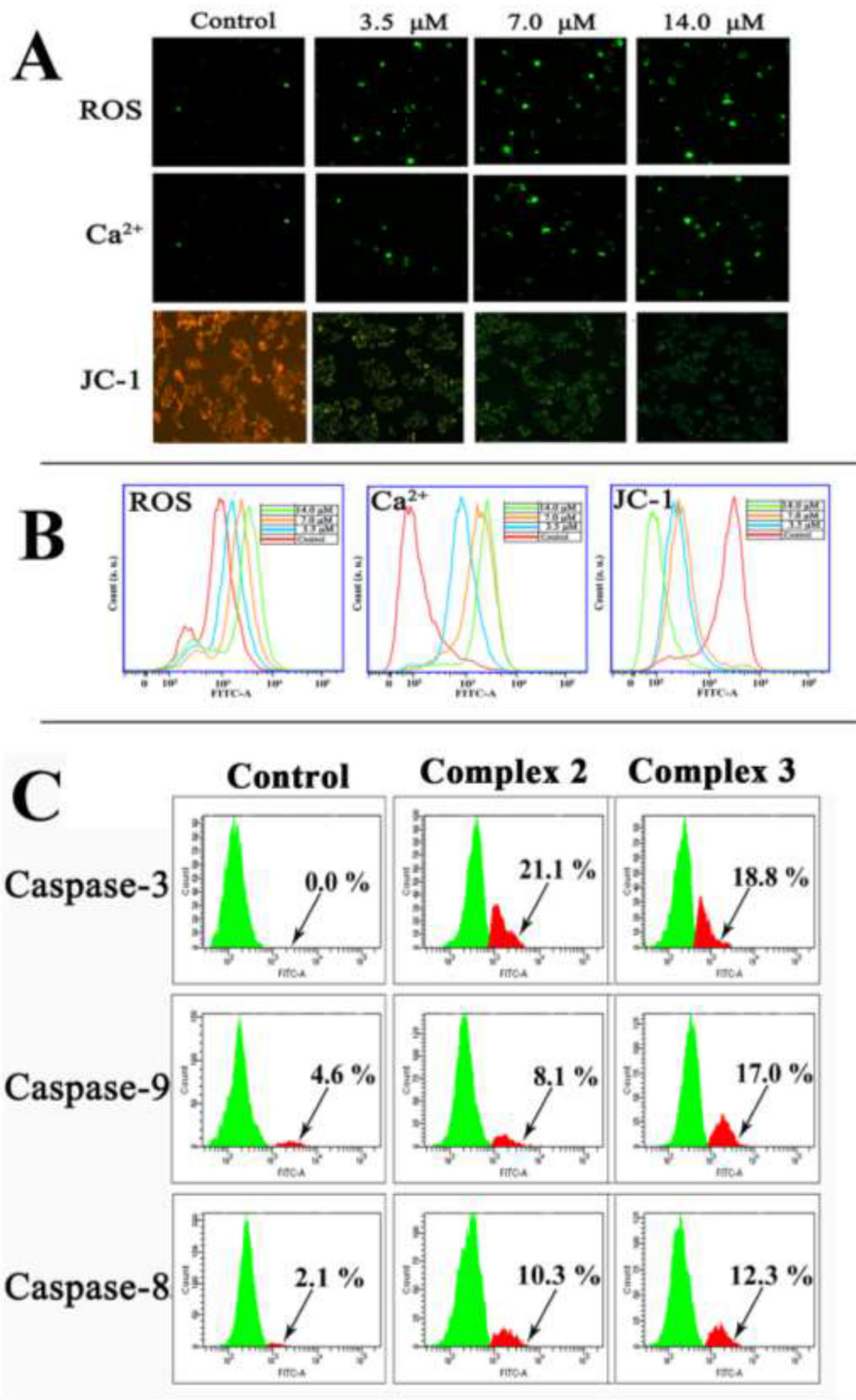


**Figure 5: The effect of 2 or 3 on the levels of ROS, intracellular Ca<sup>2+</sup>, loss of  $\Delta\Psi\text{m}$  and the activated caspase-3/8/9 expression after HepG2 cells were treated with 2 and 3 for 24 h, respectively. (A) The images of fluorescence microscope (magnification 100 $\times$ ). (B) The change of ROS, Ca<sup>2+</sup> and  $\Delta\Psi\text{m}$  examined by flow cytometry assay. (C) Flow cytometry analysis of activated caspase-3/8/9 expression in HepG2 cells after incubated with 2 and 3 at IC<sub>50</sub> values for 24 h.**

Ca<sup>2+</sup> level and the loss of ΔΨ<sub>m</sub>. Similarly, treating the HepG2 cells with **3** (7.0, 14.0 and 28.0 μM) for 24 h also caused overproduction of ROS, rising intracellular Ca<sup>2+</sup>, and loss of ΔΨ<sub>m</sub> (Supplementary Figure 6). Therefore, it is highly possible that **2** and **3** induced cell apoptosis via the mitochondrial pathway.

### Activation of caspases-3/-8/-9 in HepG2 cells

Caspases are considered to be the central executioners of cell apoptosis. The activation of caspase-3/-9 is an essential

factor in the mitochondrial apoptotic pathway [63]. The activation of caspase-3 and caspase-9 in HepG2 cells caused by **2** and **3** were analysed by flow cytometry after the cells were treated **2** and **3** at IC<sub>50</sub> for 24 h. The proportion of activated caspase-3, -9 and -8 cells after treatment with complex **2** were 21.1%, 8.1%, and 10.3% of total cells, respectively (Figure 5C). Similarly, complex **3** increased the activation of caspase-3, -9 and -8 were 18.8%, 17.0% and 12.3%, respectively. These results suggested that **2** and **3** were efficient activators of caspase-3, -9 and -8 and induced apoptosis in HepG2 cells via the caspase-dependent mitochondrial pathway.

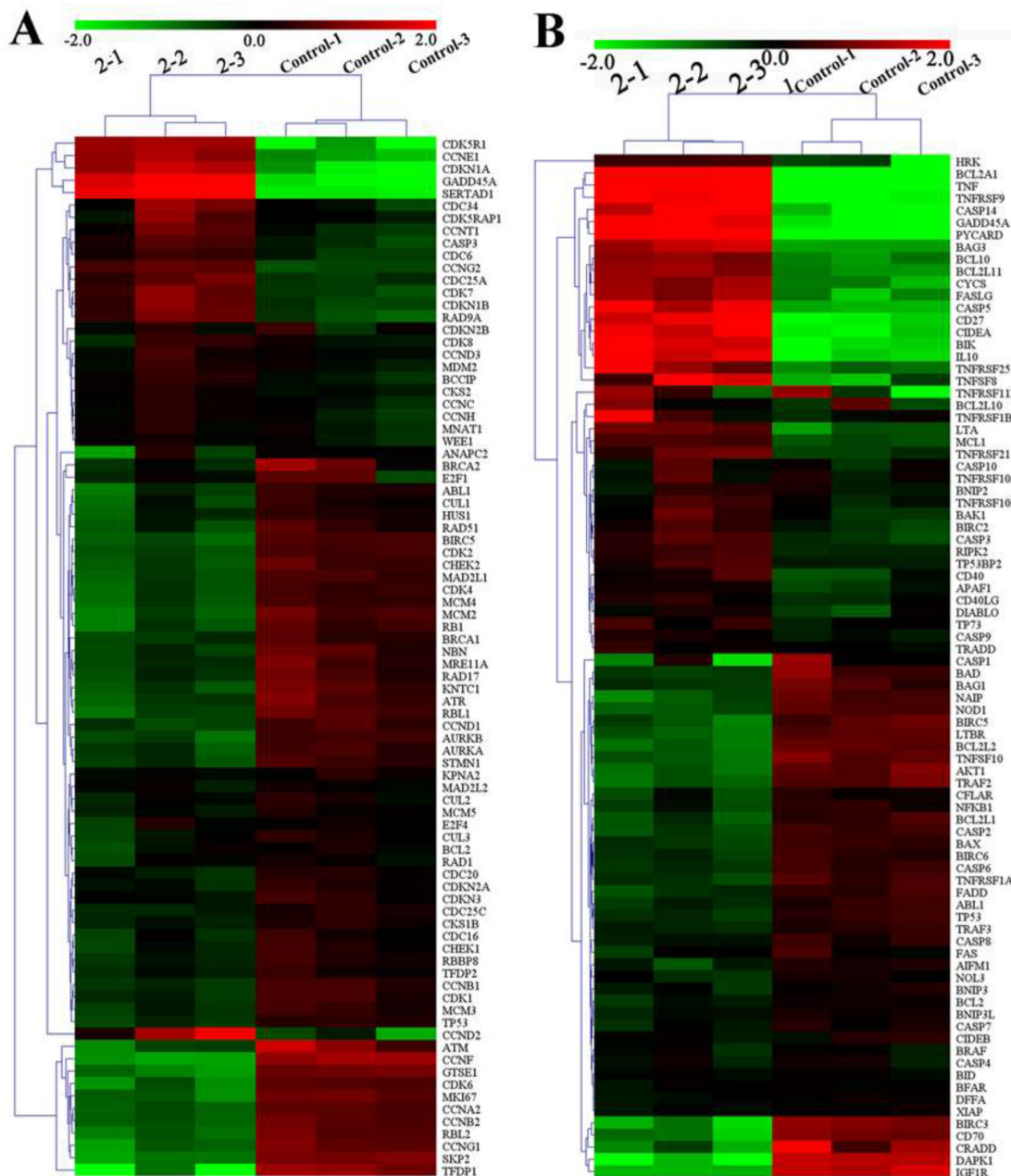


**Figure 6: Relative expression profiles of 89 genes in HepG2 cells after being treated with **2** (7.0 μM) for 24 h. (A) Cell cycle related genes and (B) apoptosis-related genes.**

## Expression of genomes related to cell cycle and apoptosis

Gene chip is widely used in screening antitumor drugs and pharmacological studies because of its high sensitivity, high flux, miniaturization, and automation [64-66]. Here we examined the expression of mRNA genes that were relevant to cell cycle and apoptosis in the HepG2 cells. Specifically, the HepG2 cells were treated with **2** (7.0  $\mu\text{M}$ ) and **3** (14.0  $\mu\text{M}$ ) for 24 h and then analyzed by

RT-qPCR array. As shown in Figure 6A, Supplementary Figure 7, Supplementary Tables 6 and 7, of the 89 cell cycle regulators genes, 58 and 31 genes were differentially expressed in mRNA levels by 1.5-fold or more after treated with **2** (7.0  $\mu\text{M}$ ) and **3** (14.0  $\mu\text{M}$ ) for 24 h, respectively. The decreased genes included CCNA2 (Cyclin A2), CCNB1 (Cyclin B1), CCND1 (Cyclin D1), CDK2, CDK6, and CHEK2 (Chk2). The activated genes included CDKN1A (p21<sup>Cip1</sup>) and CDKN1B (p27<sup>Kip1</sup>), agreed well with the protein expression results from Western blot analysis. It

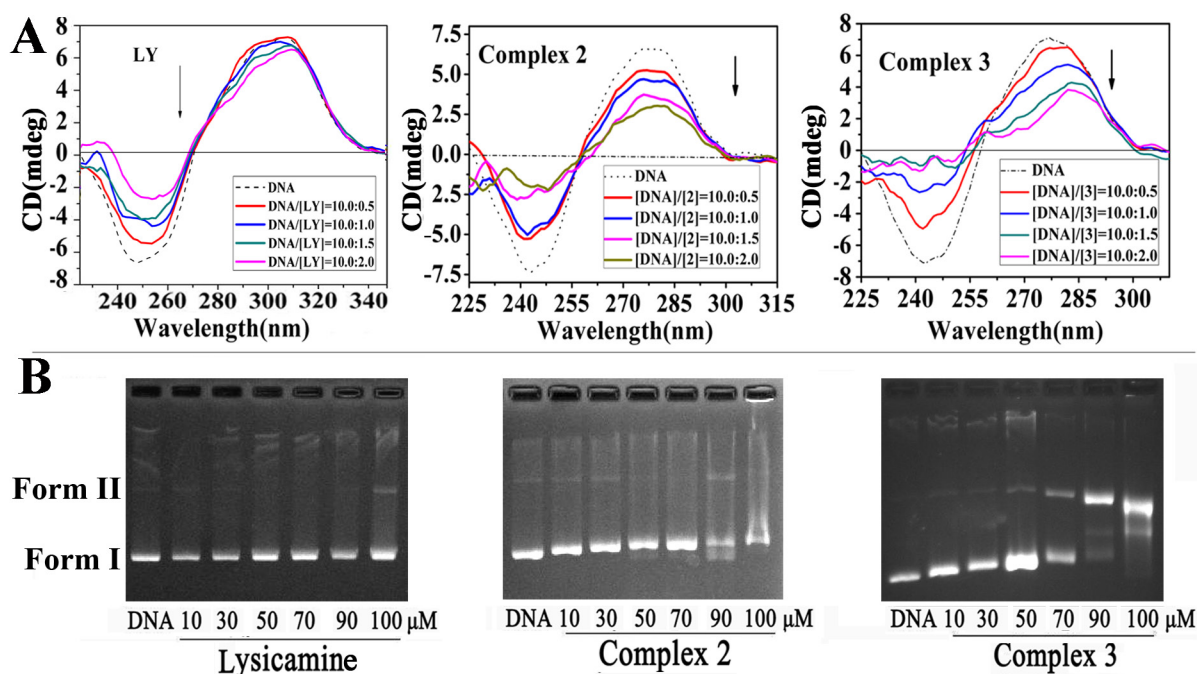


**Figure 7:** (A) Circular dichroism spectra of ct-DNA bound to LY, **2** and **3** with [DNA]/[each compound] ratios range were 10:0.5, 10:1.0, 10:1.5 and 10:2.0 (the concentration of ct-DNA bases alone of  $1 \times 10^{-4}$  M, dashed line). (B) Agarose gel electrophoresis mobility shift assay of pBR322 plasmid DNA (0.5  $\mu\text{g}/\mu\text{L}$ ) when interacted with LY, **2** and **3** with increasing concentrations from 10 to 100  $\mu\text{M}$ .

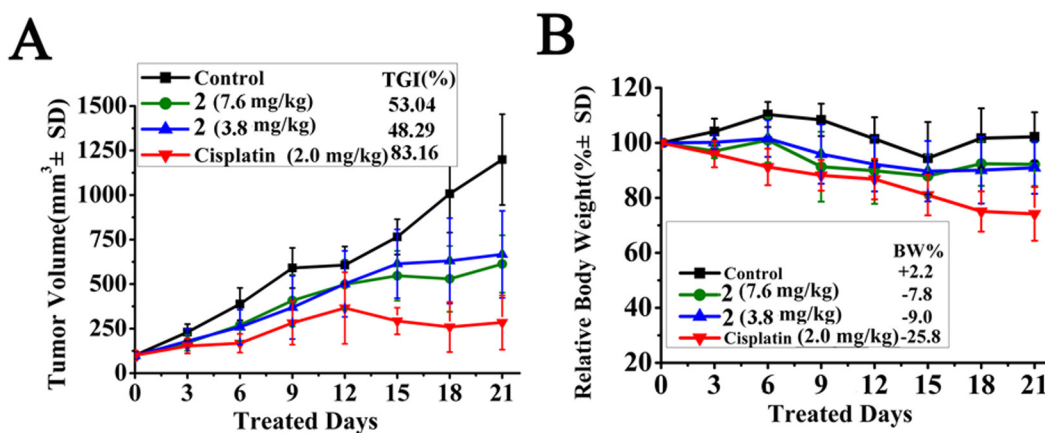


**Figure 8:** *In vivo* anticancer activity of **2** in HepG2 xenograft model. (A) Tumour volume vs days of treatment with **2** (7.6, 3.8 mg/kg/2 days), cisplatin (2.0 mg/kg/2days), or vehicle. Tumour growth is tracked by the mean tumour volume (mm<sup>3</sup>)  $\pm$  SD (n=6) and calculated as tumour growth rate [TGI%] values. (B) Body weight change. Relative body weight by considering the body weight at the start of the treatment as 100%, the percent weight loss or gain was calculated on subsequent days of treatment.

could be concluded that **2** and **3** arrested the cell cycle in the S phase by altering the expression of related genes and proteins, such as the checkpoint protein and the cyclin–Cdk complexes.

Furthermore, of the 89 apoptosis-related genes, 61 and 34 genes were differentially expressed in mRNA levels by 1.5-fold or more after treated with **2** (7.0  $\mu\text{M}$ ) and **3** (14.0  $\mu\text{M}$ ) for 24 h, respectively (Figure 6B, Supplementary Figure 8, Supplementary Tables 8 and 9). For **2**, the activated mRNA genes included CASP3, CASP9, CYCS (cytochrome *c*), and APAF1, and BCL2 was decreased. The results here again agreed well with the protein expression results from Western blot analysis. In addition, the expression levels of some mRNA genes changed significantly, e.g., TNF up to 70.12-fold, BCL2A1 up to 63.84-fold, CASP14, GADD45A, HRK, PYCARD, and TNFRSF9 up to 20.12–33.25-fold, BIK, CD27, CIDEA, and IL10 up to 12.41–13.56-fold, and DAPK1 down to 10.41-fold. Complex **3** had similar effects on the apoptosis genes, but the changes were less pronounced than in the case of **2**.

It is worth noting that tremendous changes occurred in the expression levels of death receptor genes including TNF, TNFRSF1A/1B (TNFR1/R2), TNFRSF 8, 9, 10, 21, 25, FAS, FADD and FASLG. As mentioned above, the initiator caspase-8 and the executioner caspase-3 (the downstream protein of death receptor) were activated after the cells were incubated with **2** and **3**. Therefore, it can be inferred that **2** and **3** promoted the apoptosis of tumour cells not only through the mitochondria-mediated intrinsic pathway but also through the death receptor-mediated extrinsic pathway [67].

## DNA binding studies

Many findings show that metal complexes can induce cell apoptosis by DNA damage mediated S phase cycle cell arrest [68, 69]. Since **2** and **3** caused the S phase arrest in HepG2, we found it worthy to evaluate the binding ability of **2** and **3** to DNA.

Circular dichroism (CD) is highly sensitive to the changes in the secondary structure of nucleic acids [70]. Covalent or intercalative binding may change the CD spectra of DNA by altering the tertiary structure of DNA [71]. We determined the CD spectra of ct-DNA in the presence of **2**, **3** and LY, respectively (Figure 7A). The addition of LY decreased in negative absorption evidently but changed the positive absorption only slightly. Therefore, intercalation was the most probable binding mode between LY and DNA since LY had a planar structure, and the binding was weak. In contrast, the addition of **2** or **3** caused significant hypochromism in both the negative and the positive bands of the CD spectrum, and the hypochromism intensified with rising [complex]/[DNA] ratio. The results indicated that the DNA formed a stable combination with **2** or **3** [72], and

the helicity and base stacking of the DNA were altered [73]. Obviously, compared with LY, **2** and **3** demonstrated stronger intercalative ability of to DNA, which could be attributed to the coordination of metal ions.

The DNA cleavage activity of **2**, **3** and LY were tested by agarose gel electrophoresis assay using pBR322 plasmid DNA (0.5  $\mu\text{g}/\mu\text{L}$ ) in TBE buffer (pH=8.5). Figure 7B shows that the addition of LY did not change the supercoiled DNA and its migration rate. In contrast, under the same experimental conditions, when the concentration of **2** increased from 10  $\mu\text{M}$  to 50  $\mu\text{M}$ , the mobility of supercoiled DNA (form I) was reduced, but the relaxed form (form II) was not observed. When the concentration of **2** increased further to 70  $\mu\text{M}$ , the form II DNA appeared. Almost all supercoiled DNA (form I) changed to relaxed DNA (form II) when the concentration of **2** reached 90 and 100  $\mu\text{M}$ . It could be concluded that **2** could cleave supercoiled DNA, and the coordinated metal probably played a key role in such cleavage [74]. In contrast, the cleavage of supercoiled DNA was still little even when the concentration of **3** reached 90 and 100  $\mu\text{M}$ . Hence, compared with **3**, **2** had stronger binding ability to the plasmid DNA.

## *In vivo* safety profile

The safety profile of **2** was test *in vivo* on male and female KM mice. A single intraperitoneal injection of high concentration of **2** (0.57 mg/mL in 10% DMSO) was made to KM mince at 0.4 mL/10 g (*i.e.*, 22.8 mg/kg). On the next day, some symptoms were observed, including slouching, slow movement, hair loss, anorexia, and the body weight decreased significantly in all treatment groups (15% body weight loss). There was no death of mice during the observation period (14 days), and 22.8 mg/kg was thus considered as the maximum tolerable dose (MTD) [75, 76]. However, the administration of **2** at MTD every three days led to much more serious the symptoms in the mice, including loose stools and lost their body weight significantly in these assay. Further study revealed that a single intraperitoneal injection of **2** at a reduced dose of 1/3 MTD (7.8 mg/kg) caused the KM mice to lose only <10% body weight on the next day, and the weight loss was fully recovered on day 3. When **2** was given at 1/3 MTD on every two days for 14 days, there was no animal death and the body weight of the mice grew slowly, suggesting that the dose at 1/3 MTD (*i.e.*, 7.6 mg/kg) was safe to KM mice and could be used *in vivo* xenograft studies.

## *In vivo* HepG2 xenograft study

The HepG2 xenograft model was further used to evaluate antitumor activity of **2** *in vivo*. As illustrated in Figure 8, **2** showed could inhibit tumour growth at 1/3 and 1/6 MTD (7.6 and 3.8 mg/kg per 2 days, respectively),

and the TGI [77] was approximately 53.04% and 48.29%, respectively ( $p < 0.01$ ). There was no obvious dose-dependent relationship. Although cisplatin could inhibit tumour growth more effectively than **2** in the HepG2 xenograft model (TGI = 83.16%,  $p < 0.001$ ), the administration of cisplatin caused a sharp loss in body weight (25.8%) that exceeded the permissible value (*i.e.*, 20%) [77]. In contrast, the body weight loss of the mice was much less (<10%) when they were treated with **2**. These results indicated that **2** had good antitumor activity *in vivo* when administered at 1/3 MTD and was safer than cisplatin.

## MATERIALS AND METHODS

### Synthesis and characterization of LY and complexes 1–4

#### Synthesis of compound (I)

2-Bromophenylacetic acid (0.2 mol) was dissolved in 200 mL  $\text{CHCl}_3$ , then 70 mL  $\text{SOCl}_2$  was added by slowly dropping, reflux at 75 °C for 2 h, the intermediate product was obtained after evaporate the solvent. Then, intermediate product dissolved in chloroform was slowly added to 0.2 mol 3,4-dimethoxyphenethylamine  $\text{CHCl}_3$  solution contain 300 mL saturated  $\text{NaHCO}_3$ . The mixture reacted on ice for 2 h, the chloroform layer washed three times by water, the white needle crystal of (**I**) were obtained recrystallized from methanol, yield of 80%. ESI-MS  $m/z$ : 379.2  $[\text{M}+\text{H}]^+$ ;  $^1\text{H-NMR}$  (500 MHz,  $d_6$ -DMSO):  $\delta$  8.08 (t,  $J = 5.6$  Hz, 1H), 7.60–7.56 (m, 1H), 7.33–7.28 (m, 2H), 7.20–7.16 (m,  $J = 8.0, 6.0, 3.1$  Hz, 1H), 6.84 (dd,  $J = 14.8, 5.1$  Hz, 2H), 6.73 (dd,  $J = 8.1, 2.0$  Hz, 1H), 3.74 (s, 3H,  $\text{OCH}_3$ ), 3.73 (s, 3H,  $\text{OCH}_3$ ), 3.60 (s, 2H), 3.33 (dd,  $J = 13.2, 7.0$  Hz, 2H), 2.70 (t,  $J = 7.3$  Hz, 2H).  $^{13}\text{C-NMR}$  (125 MHz,  $d_6$ -DMSO):  $\delta$  169.21, 149.11, 147.72, 136.49, 132.69, 132.38, 132.23, 129.00, 127.97, 124.94, 120.99, 113.03, 112.37, 55.99, 55.84, 42.85, 41.03, 35.17. Elemental analysis, calcd (%) for  $\text{C}_{18}\text{H}_{20}\text{BrNO}_3$ : C 57.15, H 5.33, N 3.70, O 12.69; found: C 57.27, H 5.24, N 3.68, O 12.74. (Spectra of ESI-MS and  $^1\text{H}/^{13}\text{C}$  NMR See in Supplementary Figures 9 and 10).

#### Synthesis of compound (II)

Compound (**I**) (0.2 mol) and  $\text{POCl}_3$  (60 mL) in dry toluene (300 mL) was refluxed at 85 °C for 3 h, after removal of the organic solvent, the residue dissolved in  $\text{CHCl}_3$  and adjust the pH of the solution to about 9 with ammonia. The organic layer washed with saturated  $\text{NaHCO}_3$  solution (200 mL $\times$ 2) followed by water (200 mL $\times$ 2), and concentrated under reduced pressure. The resulting residue was used for the next step without further purification. The residue was dissolved in  $\text{CH}_3\text{OH}$  and  $\text{CH}_2\text{Cl}_2$  system (v/v,1:1) and added 0.2 mol sodium triacetoxyborohydride (STAB), reacted at room temperature for 1 h, then evaporated. The residue was

dissolved in  $\text{CH}_2\text{Cl}_2$  and then wash with saturated  $\text{NaHCO}_3$  solution (200 mL $\times$ 2) followed by water (200 mL $\times$ 2). The residue was purified through recrystallized from ethanol to afford compound (**II**), yield of 82 %. ESI-MS  $m/z$ : 362.3  $[\text{M}+\text{H}]^+$ ;  $^1\text{H NMR}$  (500 MHz,  $\text{CDCl}_3$ ):  $\delta$  7.56 (d,  $J = 7.8$  Hz, 1H), 7.26–7.23 (m, 2H), 7.14–7.10 (m, 1H), 6.58 (s, 1H), 6.27 (s, 1H), 4.50 (t,  $J = 7.1$  Hz, 1H), 3.83 (s, 3H,  $\text{OCH}_3$ ), 3.62 (s, 3H,  $\text{OCH}_3$ ), 3.41–3.17 (m, 4H), 2.93–2.86 (m, 2H), 1.86 (s, 1H, NH);  $^{13}\text{CNMR}$  (125 MHz,  $\text{CDCl}_3$ ):  $\delta$  176.82, 148.08, 147.08, 137.08, 133.05, 132.35, 128.66, 127.66, 126.56, 125.20, 111.42, 109.78, 55.81, 55.64, 54.06, 41.73, 38.77, 27.04; Elemental analysis, calcd (%) for  $\text{C}_{18}\text{H}_{20}\text{BrNO}_2$ : C 59.68, H 5.56, N 3.87, O 8.83; found: C 59.61, H 5.47, N 3.92, O 8.84. (Spectra of ESI-MS and  $^1\text{H}/^{13}\text{C}$  NMR See in Supplementary Figures 11 and 12).

#### Synthesis of compound (III)

The 0.2 mol compound (**II**) dissolved in 150 mL  $\text{CHCl}_3$  and added  $\text{NaOH}$  solution (0.2mol/L), stirring, then 0.2 mol  $\text{ClCOOCH}_3$  (dissolved in  $\text{CHCl}_3$ ) was slowly added. The mixture keep stirring on ice for 1 h, then the organic layer washed with water two times, and concentrated under reduced pressure. The residue recrystallized in methanol, and the white needle crystal (**III**) were obtained, yield of 88%. ESI-MS  $m/z$ : 419.3  $[\text{M}-\text{H}]^-$ ;  $^1\text{H NMR}$  (500 MHz,  $d_6$ -DMSO):  $\delta$  7.69–7.65 (m, 1H), 7.28–7.22 (m, 1H), 7.18–7.15 (m, 1H), 7.00 (s, 1H), 6.82 (d,  $J = 5.8$  Hz, 1H), 6.78 (s, 1H), 3.84 (s, 3H,  $\text{OCH}_3$ ), 3.78 (s, 3H,  $\text{OCH}_3$ ), 3.74 (s, 3H,  $\text{OCH}_3$ ), 3.72–3.70 (m, 3H), 3.15–3.09 (m, 4H), 2.83 (d,  $J = 6.3$  Hz, 2H).  $^{13}\text{C NMR}$  (125 MHz,  $d_6$ -DMSO):  $\delta$  155.08, 149.97, 148.08, 146.46, 133.01, 132.68, 130.09, 129.54, 129.29, 128.88, 128.3, 112.54, 107.30, 56.25, 55.97, 55.85, 55.03, 53.21, 44.55, 43.81, 28.47. Elemental analysis, calcd (%) for  $\text{C}_{20}\text{H}_{22}\text{BrNO}_4$ : C 57.15, H 7.28, N 3.33, O 15.23; found: C 57.21, H 7.21, N 3.40, O 15.30. (Spectra of ESI-MS and  $^1\text{H}/^{13}\text{C}$  NMR See in Supplementary Figures 13 and 14).

#### Synthesis of compound (IV)

10.0 g compound (**III**), 1.4 g tricyclohexyl phosphine, 11.5 g  $\text{K}_2\text{CO}_3$  and 0.53 g  $\text{Pd}(\text{Ac})_2$  were dissolved in dry DMA, the suspension was heated to 135 °C under  $\text{N}_2$  for 5 h. After the completion of the reaction (monitored by TLC), DMA was distilled off under high vacuum, and the residue was dissolved in chloroform (200 mL) and washed with saturated  $\text{NaHCO}_3$  solution (100 mL $\times$ 2), followed by water (100 mL $\times$ 2). The organic layer was concentrated under reduced pressure and purified though recrystallized in methanol, the white needle crystal (compound IV) were obtained, yield of 84%. ESI-MS  $m/z$ : 339.4  $[\text{M}+\text{H}]^+$ ;  $^1\text{H NMR}$  (500 MHz,  $\text{CDCl}_3$ ):  $\delta$  8.46 (d,  $J = 7.9$  Hz, 1H), 7.37–7.33 (m, 1H), 7.28 (d,  $J = 3.4$  Hz, 2H), 6.70 (s, 1H), 3.92 (s, 3H,  $\text{OCH}_3$ ), 3.78 (s, 3H,  $\text{OCH}_3$ ), 3.68 (s, 3H,  $\text{OCH}_3$ ), 3.28–3.20 (m, 1H), 3.03–2.84 (m, 4H), 2.02–1.89 (m, 2H);  $^{13}\text{CNMR}$  (125 MHz,  $\text{CDCl}_3$ ):  $\delta$  152.08, 150.96, 145.65, 136.77, 131.70, 128.49, 128.38, 127.68, 127.04, 126.68, 126.13, 125.87,

111.48, 60.04, 56.47, 55.95, 43.33, 38.93, 30.21, 27.64; Elemental analysis, calcd (%) for  $C_{20}H_{21}NO_4$ : C, 70.78; H, 6.24; N, 4.13; O, 18.86; found: C, 70.83; H, 6.21; N, 4.20; O, 18.21. (Spectra of ESI-MS and  $^1H$ / $^{13}C$  NMR See in Supplementary Figures 15 and 16).

### Synthesis of compound (V)

8.8g compound (IV) and 8.0 g  $LiAlH_4$  were dissolved in dry THF (600 mL) under  $N_2$  on ice, then the suspension heated to 65°C for 5 h. After removal of THF, the residue was dissolved in ethyl acetate, and ammonia was added until no bubbles on the ice bath. The organic layer was concentrated under reduced pressure and purified though recrystallized in methanol, the blackish green needle crystal (compound V) were obtained, yield of 56%. ESI-MS m/z: 296.3[M+H]<sup>+</sup>;  $^1H$  NMR (500 MHz,  $CDCl_3$ ):  $\delta$  8.40 (d,  $J$  = 7.8 Hz, 1H), 7.34 (t,  $J$  = 7.1 Hz, 1H), 7.30–7.24 (m, 2H), 6.66 (s, 1H), 3.91 (s, 3H,  $OCH_3$ ), 3.68 (s, 3H,  $OCH_3$ ), 3.20–3.06 (m, 4H), 2.74–2.65 (m, 2H), 2.58 (s, 3H,  $CH_3$ ), 2.55–2.52 (m, 1H);  $^{13}C$  NMR (125 MHz,  $CDCl_3$ ):  $\delta$  152.04, 145.18, 136.41, 132.14, 128.66, 128.34, 127.89, 127.83, 127.36, 1127.03, 126.90, 111.29, 62.34, 60.25, 55.87, 53.28, 43.93, 35.08, 29.16; Elemental analysis, calcd (%) for  $C_{19}H_{21}NO_2$ : C 77.26, H 7.17, N 4.74, O 10.83; found: C 77.28, H 7.11, N 4.76, O 10.89. (See in Supplementary Figures 17 and 18).

### Synthesis of lysicamine (LY)

0.02 mol compound (V) and 0.7 mol  $Mn(Ac)_3$  were dissolved in 500 mL glacial acetic acid, 80 °C reflux for 12 h(monitored by TLC). Glacial acetic acid was distilled off under high vacuum, and the residue was purified though recrystallized from methanol, purification by silica gel chromatography ( $CH_2Cl_2/MeOH/NH_3(aq)$  = 98:1:1), the blackish green crystal (Lysicamine) were obtained, yield of 23%. ESI-MS m/z: 292.1 [M+H]<sup>+</sup>;  $^1H$  NMR (500 MHz,  $d_6$ -DMSO):  $\delta$  9.14 (d,  $J$  = 8.3 Hz, 1H), 8.86 (d,  $J$  = 5.3 Hz, 1H), 8.38 (d,  $J$  = 7.7 Hz, 1H), 8.17 (d,  $J$  = 5.3 Hz, 1H), 7.91 (t,  $J$  = 7.8 Hz, 1H), 7.76 (s, 1H), 7.68 (t,  $J$  = 7.5 Hz, 1H), 4.10 (s, 3H), 4.02 (s, 3H);  $^{13}C$  NMR (125 MHz,  $d_6$ -DMSO):  $\delta$  182.03, 156.96, 152.57, 145.08, 135.71, 135.13, 134.37, 131.99, 129.41, 129.10, 128.71, 128.45, 124.71, 121.93, 118.61, 108.30, 60.93, 56.90; Elemental analysis, calcd (%) for  $C_{18}H_{13}NO_3$ : C 74.22, H 4.50, N 4.81, O 16.48; found: C 74.25, H 4.46, N 4.77, O 16.53. (Spectra of ESI-MS and  $^1H$ / $^{13}C$  NMR See in Supplementary Figures 19 and 20).

### Synthesis of 1–4

#### Synthesis of $[Ru(LY)Cl_2(DMSO)_2] \cdot 3H_2O$ (1)

Cis- $RuCl_2(DMSO)_4$  was repaired according the report [78], 1.0 mmol LY (0.0146 g) and 0.1 mmol cis- $RuCl_2(DMSO)_4$  (0.049 g) were dissolved in  $CHCl_3CH_3OH$  solution (v/v,1:1), reflux for 12 h in 65 °C water bath, then cooling and filter, the filtrated solution was allowed to

evaporate slowly for a week, green block crystals suitable for X-ray single-crystal diffraction analysis were harvested, yield of 50%. IR(KBr): (-NH) 3452 (m), (Ar-H) 3008 (m), (C=O) 1601 (m), (C=C) 1563, 1481, 1468 (s), (C-O) 1412, 1269 (vs), (C-N) 1026 (s)  $cm^{-1}$ ; ESI-MS m/z: 619 [M+H]<sup>+</sup>, 652 [M+CH<sub>3</sub>OH+H]<sup>+</sup>; Elemental analysis, calcd (%) for  $C_{22}H_{31}Cl_2NO_8RuS_2$ : C, 42.88; H, 3.755; N, 2.29; Found. C, 42.65; H, 4.07; N, 2.26. (Spectra of ESI-MS See in Supplementary Figure 21).

#### Synthesis of $[Rh(LY-OH)Cl_3CH_3OH] \cdot H_2O$ (2)

LY (0.1 mmol, 0.0146g), 0.1 mmol  $RhCl_3 \cdot 3H_2O$  (0.0209 g), methanol (1.0 mL), chloroform (1.0 mL) were placed in a thick Pyrex tube (ca 20 cm long), the mixture was frozen by liquid  $N_2$ , and then evacuated under vacuum and sealed. Then it was heated at 80 °C for 72 h. Then the dark red bulk crystals suitable for single-crystal X-ray diffraction analysis were harvested, about yield of 56%. IR(KBr): (-NH) 3357 (m), (Ar-H) 3066 (m), (C=O) 1602 (m), (C=C) 1557, 1496, 1429 (s), (C-O)1278 1214(vs), (C-N) 1077 (s)  $cm^{-1}$ ; ESI-MS m/z: 516.81, [M-H]<sup>-</sup>; Elemental analysis, calcd (%) for  $C_{18}H_{15}Cl_3NO_5Rh$ : C, 40.58; H, 2.724; N, 2.81; Found. C, 41.86; H, 2.735; N, 2.72;  $^1H$  NMR (500 MHz,  $d_6$ -DMSO):  $\delta$  10.02 (d,  $J$  = 8.7 Hz, 1H), 9.24 (d,  $J$  = 5.3 Hz, 1H), 8.54 (d,  $J$  = 7.3 Hz, 1H), 8.22 (d,  $J$  = 5.4 Hz, 1H), 7.91 (s, 1H), 7.59 (s, 1H), 7.37 (s, 1H), 4.01 (s, 3H).  $^{13}C$  NMR (125 MHz,  $d_6$ -DMSO):  $\delta$  181.52, 173.11, 159.32, 143.94, 138.45, 136.69, 136.65, 134.38, 127.14, 126.18, 125.43, 124.81, 124.70, 123.94, 107.74, 105.41, 56.52, 49.08. (Spectra of ESI-MS and  $^1H$ / $^{13}C$  NMR See in Supplementary Figures 22-24).

#### Synthesis of $[Mn(LY)_3](ClO_4)_2 \cdot 3(CHCl_3)(3)$

The same method was employed by 2, yield of 68%. IR(KBr): (-NH) 3424(m), (Ar-H) 2942(m), (C=O) 1609(m), (C=C) 1588, 1480, 1466(s), (C-O) 1412, 1269(vs), (C-N) 1096(s)  $cm^{-1}$ ; ESI-MS m/z: 1027.05, [M- $ClO_4$ ]<sup>+</sup>; Anal. Calcd (%), for  $C_{56}H_{41}Cl_8MnN_3O_{17}$ : C 56.63, H 3.469, N 3.65; Found. C 56.54, H 3.49, N 3.73. (Spectra of ESI-MS See in Supplementary Figure 25).

#### Synthesis of $[Zn(LY)_2(ClO_4)_2] (4)$

The same method was employed by 2, yield of 60%. IR(KBr):(-NH) 3438(m), (Ar-H) 2944(m), (C=O) 1608(m), (C=C) 1578, 1482, 1467(s), (C-O)1412, 1275(vs), (C-N) 1045(s)  $cm^{-1}$ ; ESI-MS m/z: 745.05, [M- $ClO_4$ ]<sup>+</sup> (Supplementary Figure 26); Anal. Calcd (%), for  $C_{36}H_{26}Cl_2ZnN_2O_{14}$ : C 50.65, H 2.96, N 3.14; Found. C 50.81, H 3.10, N 3.32.

### X-ray crystallography

The instrument and the method of single-crystal X-ray diffraction analysis was performed as our previously reports [13, 55, 66]. The CCDC numbers for complexes 1–4 are CCDC 1543054-1543057.

## Materials and other methods

All the materials, instrumentation, and the detailed procedures for other experimental methods are described in supporting information.

## CONCLUSIONS

In summary, we have developed a facile concise synthesis of lysicamine from simple raw materials under mild conditions. This successful synthesis could shed light on the preparation of other oxoaporphine alkaloids.

Four new metal complexes **1–4** of lysicamine (LY) were made and fully characterized. The complexes exhibit *in vitro* cytotoxicity to selected tumour cells. In particular, **2** and **3** showed high antitumor activity to HepG2 and NCI-H460 cells. Mechanistic studies showed that **2** and **3** blocked cell cycle at the S phase by increasing the expression of p53, p21, p27, and Cdc25A, as well as decreasing the expression of cyclin A2, cyclin B1, cyclin D1, cyclin E1, CDK2, CDK6 and PCNA. Besides, **2** and **3** also induced cell apoptosis by up-regulating Bax, Apaf-1, cytochrome *c* and down-regulating c-myc and Bcl-2. In addition, **2** and **3** also promoted ROS production, increased intracellular Ca<sup>2+</sup>, enhanced  $\Delta\psi$  loss, and triggered caspase-3/-8/-9 activation. These results suggested that **2** and **3** mediated apoptosis via the caspase-dependent mitochondrial pathway. Gene chip experiments showed that **2** notably changed the expression levels of genes associated with death receptors, and indicated that **2** also induced apoptosis via the death receptor pathway. Furthermore, **2** inhibited HepG2 tumour growth *in vivo*, and showed better safety profile than cisplatin. In conclusion, this work confirmed that **2** and **3** had high antitumor activity towards HepG2 cells, and that **2** could be a promising candidate to be further developed into an effective antitumor agent.

## ACKNOWLEDGMENTS

This work was supported by the National Natural Science Foundation of China (Grants 81473102, 21431001), CMEMR2012-A22, IRT\_16R15 and the Natural Science Foundation of Guangxi Province of China (No. 2016GXNSFGA380005) as well as “BAGUI Scholar” program of Guangxi Province of China. Microarray experiments of telomeres/telomerase-related genes expression were performed by KangChen Bio-tech, Shanghai, China.

## CONFLICTS OF INTEREST

The authors declared that they have no conflicts of interest to this work.

## REFERENCES

1. Jantan I, Raweh SM, Yasin YH, Murad S. Antiplatelet activity of aporphine and phenanthrenoid alkaloids from *Aromadendron elegans* Blume. *Phytother Res.* 2006; 20: 493–496.
2. Remichkova M, Dimitrova P, Philipov S, Ivanovska N. Toll-like receptor-mediated anti-inflammatory action of glaucine and oxoglucine. *Fitoterapia.* 2009; 80: 411–414.
3. Wirasathien L, Boonarkart C, Pengsuparp T, Suttisri R. Biological activities of alkaloids from *Pseuduvaria setosa*. *Pharm Biol.* 2006; 44: 274–278.
4. Yang CH, Cheng MJ, Lee SJ, Yang CW, Chang HS, Chen IS. Secondary metabolites and cytotoxic activities from the stem bark of *Zanthoxylum nitidum*. *Chem Biodivers.* 2009; 6: 846–857.
5. Hsieh TJ, Liu TZ, Chern CL, Tsao DA, Lu FJ, Syu YH, Hsieh PY, Hu HS, Chang TT, Chen CH. Liriodenine inhibits the proliferation of human hepatoma cell lines by blocking cell cycle progression and nitric oxide-mediated activation of p53 expression. *Food Chem Toxicol.* 2005; 43: 1117–1126.
6. Pai BR, Shanmugasundaram G. Synthesis of atherospermidine. *Tetrahedron.* 1965; 21: 2579–2584.
7. Saá C, Guitián E, Castedo L, Saá JM. The intermolecular benzyne cycloaddition approach to dehydronoraporphines and oxoaporphines. Total synthesis of PO-3. *Tetrahedron Lett.* 1985; 26: 4559–4560.
8. Atanes N, Castedo L, Guitián E, Saá C, Saá JM. Intermolecular benzyne cycloaddition (IBC) approach to aporphinoids. Total syntheses of norcepharadione B, cepharadione B, dehydroanonaine, duguenaïne, dehydronormuciferine, pontevedrine, O-methylatheroline, lysicamine, and alkaloid PO-3. *J. Org Chem.* 1991; 56: 2984–2988.
9. Castedo L, Suau R, Mourino A. Isoquinoline alkaloids. 4. Simple entry to oxoaporphine alkaloids-corunnine and glauvine. *Heterocycles.* 1975; 3: 449–451.
10. LeGendre O, Pecic S, Chaudhary S, Zimmerman SM, Fantegrossi WE, Harding WW. Synthetic studies and pharmacological evaluations on the MDMA (‘Ecstasy’) antagonist nantenine. *Bioorg Med Chem Lett.* 2010; 20: 628–631.
11. Singh OV, Huang WJ, Chen CH, Lee SS. Manganese(III) acetate mediated oxidation of aporphines: a convenient and useful synthesis of oxoaporphines. *Tetrahedron Lett.* 2007; 48: 8166–8169.
12. Chen ZF, Shi YF, Liu YC, Hong X, Geng B, Peng Y, Liang H. TCM active ingredient oxoglucine metal complexes: crystal structure, cytotoxicity, and interaction with DNA. *Inorg Chem.* 2012; 51: 1998–2009.
13. Wei JH, Chen ZF, Qin JL, Liu YC, Li ZQ, Khan TM, Wang M, Jiang YH, Shen WY, Liang H. Water-soluble oxoglucine-Y(III), Dy(III) complexes: *in vitro* and *in vivo*

- anticancer activities by triggering DNA damage, leading to S phase arrest and apoptosis. *Dalton Trans.* 2015; 44: 11408–11419.
14. Hella M, Singh S, Cuny GD. Monoligated Pd (0)-catalyzed intramolecular ortho- and para-arylation of phenols for the synthesis of aporphine alkaloids. Synthesis of (–)-lirinine. *Tetrahedron.* 2012; 68: 1674–1681.
  15. Resch V, Lechner H, Schrittwieser JH, Wallner S, Gruber K, Macheroux P, Kroutil W. Inverting the regioselectivity of the berberine bridge enzyme by employing customized fluorine-containing substrates. *Chem Eur J.* 2012; 18: 13173–13179.
  16. Rossini AF, Muraca AC, Casagrande GA, Raminelli C. Total syntheses of aporphine alkaloids via benzyne chemistry: an approach to the formation of aporphine cores. *J Org Chem.* 2015; 80: 10033–10040.
  17. Santini C, Pellei M, Gandin V, Porchia M, Tisato F, Marzano C. Advances in copper complexes as anticancer agents. *Chem Rev.* 2014; 114: 815–862.
  18. Heidary DK, Howerton BS, Glazer EC. Coordination of hydroxyquinolines to a ruthenium bis-dimethylphenanthroline scaffold radically improves potency for potential as antineoplastic agents. *J Med Chem.* 2014; 57: 8936–8946.
  19. Redemaker-Lakhai JM, van den Bongard D, Pluim D, Beijnen JH, Schellens JH. A Phase I and pharmacological study with imidazolium-trans-DMSO-imidazole-tetrachlororuthenate, a novel ruthenium anticancer agent. *Clin Cancer Res.* 2004; 10: 3717–3727.
  20. Reisner E, Arion VB, Guedes da Silva MF, Lichteneker R, Eichinger A, Keppler BK, Kukushkin VY, Pombeiro AJ. Tuning of redox potentials for the design of ruthenium anticancer drugs—an electrochemical study of [*trans*-RuCl<sub>4</sub>L(DMSO)]- and [*trans*-RuCl<sub>4</sub>L<sub>2</sub>]-complexes, where L= imidazole, 1,2,4-triazole, indazole. *Inorg Chem.* 2004; 43: 7083–7093.
  21. Bergamo A, Sava G. Ruthenium anticancer compounds: myths and realities of the emerging metal-based drugs. *Dalton Trans.* 2011; 40: 7817–7823.
  22. Zhang HR, Liu YC, Chen ZF, Meng T, Zou BQ, Liu YN, Liang H. Studies on the structures, cytotoxicity and apoptosis mechanism of 8-hydroxyquinoline rhodium(III) complexes in T-24 cells. *New J Chem.* 2016; 4: 6005–6014.
  23. Ruiz J, Rodríguez V, Cutillas N, Samper KG, Palacios MC, Espinosa A. Novel C,N-chelate rhodium(III) and iridium(III) antitumor complexes incorporating a lipophilic steroidal conjugate and their interaction with DNA. *Dalton Trans.* 2012; 41: 12847–12856.
  24. Śliwińska U, Pruchnik FP, Pelińska I, Ułaszewski S, Wilczok A, Zajdel A. Synthesis, structure and antitumor activity of [RhCl<sub>3</sub>(N–N)(DMSO)] polypyridyl complexes. *J Inorg Biochem.* 2008; 102: 1947–1951.
  25. Zhang JJ, Muenzner JK, el Maaty MA, Karge B, Chobert RS, Wölfl S. A multi-target caffeine derived rhodium(I) N-heterocyclic carbene complex: evaluation of the mechanism of action. *Dalton Trans.* 2016; 45: 13161–13168.
  26. Siu FM, Lin IW, Yan K, Lok CN, Low KH, Leung TY, Lam TL, Che CM. Anticancer dirhodium(ii,ii) carboxylates as potent inhibitors of ubiquitin-proteasome system. *Chem Sci.* 2012; 3: 1785–1793.
  27. Liu YC, Wei JH, Chen ZF, Liu M, Gu YQ, Wang, KB, Li ZQ, Liang H. The antitumor activity of zinc(II) and copper(II) complexes with 5, 7-dihalo-substituted-8-quinolinoline. *Eur J Med Chem.* 2013; 69: 554–563.
  28. Gauna GA, Marino J, Vior MC, Roguin LP, Awruch J. Synthesis and comparative photodynamic properties of two isosteric alkyl substituted zinc(II) phthalocyanines. *Eur J Med Chem.* 2011; 46: 5532–5539.
  29. Enyedy EA, Nagy NV, Zsigo E, Kowol CR, Arion VB, Keppler BK, Kiss T. Comparative solution equilibrium study of the interactions of copper(II), iron(II) and zinc(II) with triapine (3-aminopyridine-2-carbaldehyde thiosemicarbazone) and related ligands. *Eur J Inorg Chem.* 2010; 11: 1717–1728.
  30. Mandal B, Singha S, Dey SK, Mazumdar S, Mondal TK, Karmakar P, Kumar S, Das S. Synthesis, crystal structure from PXRD of a Mn<sup>II</sup>(purp)<sub>2</sub> complex, interaction with DNA at different temperatures and pH and lack of stimulated ROS formation by the complex. *RSC Adv.* 2016; 6: 51520–51532.
  31. Chen J, Zhang W, Zhang M, Guo Z, Wang H, He M, Xu P, Zhou JJ, Liu Z, Chen Q. Mn(II) mediated degradation of artemisinin based on Fe<sub>3</sub>O<sub>4</sub>@ MnSiO<sub>3</sub>-FAnanospheres for cancer therapy *in vivo*. *Nanoscale.* 2015; 7: 12542–12551.
  32. Chen ZF, Liang H. Progresses in TCM metal-based antitumor agents. *Anticancer Agents Med Chem.* 2010; 10: 412–423.
  33. Liu YC, Chen ZF, Liu LM, Peng Y, Hong X, Yang B, Liu HG, Liang H, Orvig C. Divalent later transition metal complexes of the traditional chinese medicine(TCM) lirioidenine: coordination chemistry, cytotoxicity and DNA binding studies. *Dalton Trans.* 2009; 48: 10813–10823.
  34. Chen ZF, Liu YC, Liu LM, Wang HS, Qin SH, Wang BL, Bian HD, Yang B, Fun HK, Liu HG, Liang H, Orvig C. Potential new inorganic antitumor agents from combining the anticancer traditional Chinese medicine (TCM) lirioidenine with metal ions, and DNA binding studies. *Dalton Trans.* 2009; 2: 262–272.
  35. Qin QP, Qin JL, Meng T, Yang GA, Wei ZZ, Liu YC, Liang H, Chen ZF. Preparation of 6/8/11-amino/chloro-oxoisorphine and group-10 metal complexes and evaluation of their *in vitro* and *in vivo* antitumor activity. *Sci Rep.* 2016; 6: 37644.
  36. Qin JL, Qin QP, Wei ZZ, Yu YC, Meng T, Wu CX, Liang YL, Liang H, Chen ZF. Stabilization of c-myc G-Quadruplex DNA, inhibition of telomerase activity, disruption of mitochondrial functions and tumor

- cellapoptosis by platinum(II) complex with 9-amino-oxoisoaporphine. *Eur J Med Chem.* 2016; 124: 417–427.
37. Hsieh J, Chang FR, Chia YC, Chen CY, Chiu HF. Cytotoxic constituents of the fruits of *Cananga odorata*. *J Nat Prod.* 2001; 64: 616–619.
  38. Ishitsuka DN, Kamikawa M, Matsuda M, Tsuchihashi R, Okawa M, Okabe H, Tamura K, Kinjo J. Screening of promising chemotherapeutic candidates from plants against human adult T-cell leukemia/lymphoma(III). *J Nat Med.* 2013; 67: 894–903.
  39. Huang KB, Chen ZF, Liu YC, Wang M, Wei JH, Xie XL, Zhang JL, Hu K, Liang H. Copper(II/I) complexes of 5-pyridin-2-yl-[1, 3] dioxolo [4,5-g] isoquinoline: Synthesis, crystal structure, antitumor activity and DNA interaction. *Eur J Med Chem.* 2013; 70: 640–648.
  40. Xu X, Guo S, Dang Q, Chen J, Bai X. A new strategy toward fused-pyridine heterocyclic scaffolds: Bischler-Napieralski-type cyclization, followed by sulfoxide extrusion reaction. *J Comb Chem.* 2007; 9: 773–782.
  41. Orito K, Uchiito S, Satoh Y, Tatsuzawa T, Harada R, Tokuda M. Aryl radical cyclizations of 1-(2'-bromobenzyl) isoquinolines with AIBN-Bu<sub>3</sub>SnH: formation of aporphines and indolo[2,1-a]isoquinolines. *Org Lett.* 2000; 2: 307–310.
  42. Estévez JC, Villaverde MC, Estévez RJ, Castedo L. Radical cyclization to aporphines. A new, efficient total synthesis of the aporphine glaucine and the 4,5-dioxoaporphine pontevedrine, and the first total synthesis of 5-oxoaporphines. *Tetrahedron.* 1994; 50: 2107–2114.
  43. Nimgirawath S, Udomputtimekakul P, Pongphuttichai S, Wanbanjob A, Taechowisan T. Total synthesis and antimicrobial activity of (±)-laurelliptinhexadecan-1-one and (±)-laurelliptinooctadecan-1-one. *Molecules.* 2008; 13: 2935–2947.
  44. Estévez JC, Villaverde M, Estévez RJ, Castedo L. Radical cyclization to dibenzo [de, g] chromanones. A new synthesis of phenanthrene compounds. *Tetrahedron* 1993; 49: 2783–2790.
  45. Chaudhary S, Pecic S, LeGendre O, Navarro HA, Harding WW. (±)-Nantenine analogs as antagonists at human 5-HT 2A receptors: C1 and flexible congeners. *Bioorg Med Chem Lett.* 2009; 19: 2530–2532.
  46. Fei H, Cao R, Jia JL, Ma XC, Zhou M. Membrane localized iridium(III) complex induces endoplasmic reticulum stress and mitochondria-mediated apoptosis in human cancer cells. *J Med Chem.* 2013; 56: 3636–3644.
  47. Wang H, Wang B, Wang M, Zheng LN, Chen HQ, Chai ZF, Zhao YL, Feng WY. Time-resolved ICP-MS analysis of mineral element contents and distribution patterns in single cells. *Analyst.* 2015; 140: 523–531.
  48. Hotamisligil GS. Endoplasmic reticulum stress and the inflammatory basis of metabolic disease. *Cell.* 2010; 140: 900–917.
  49. Schreiber E, Matthias P, Muellerand MM, Schaffner W. Rapid detection of octamer binding proteins with 'mini-extracts', prepared from a small number of cells. *Nucleic Acids Res.* 1989; 17: 6419.
  50. Zurlo D, Leone C, Assante G, Salzano S, Renzone G, Scaloni A, Foresta C, Colantuoni V, Lupo A. Cladosporol a stimulates G1-phase arrest of the cell cycle by up-regulation of p21<sup>waf1/cip1</sup> expression in human colon carcinoma HT-29 cells. *Mol Carcinog.* 2013; 52: 1–17.
  51. Chilampalli C, Guillermo R, Kaushik RS, YoungA, Chandrasekher G, Fahmy H, Dwivedi C. Honokiol, a chemopreventive agent against skin cancer, induces cell cycle arrest and apoptosis in human epidermoid A431 cells. *Exp Biol Med.* 2011; 236: 1351–1359.
  52. Lee YS, Choi KM, Kim W, Jeon YS, Lee YM, Hong JT, Yun YP, Yoo HS. Hinokitiol inhibits cell growth through induction of S-phase arrest and apoptosis in human colon cancer cells and suppresses tumor growth in a mouse xenograft experiment. *J Nat Prod.* 2013; 76: 2195–2202.
  53. Mailand N, Gibbs-Seymour I, Bekker-Jensen S. Regulation of PCNA-protein interactions for genome stability. *Nat Rev Mol Cell Biol.* 2013; 14: 269–282.
  54. Hsu JD, Kao SH, Ou TT, Chen YJ, Li YJ, Wang CJ. Gallic acid induces G2/M phase arrest of breast cancer cell MCF-7 through stabilization of p27<sup>KIP1</sup> attributed to disruption of p27Kip1/Skp2 complex. *J Agric Food Chem.* 2011; 59: 1996–2003.
  55. Qin QP, Liu YC, Wang HL, Qin JL, Cheng FJ, Tang SF, Liang H. Synthesis and antitumor mechanisms of a copper(II) complex of anthracene-9-imidazoline hydrazone (9-AIH). *Metallomics.* 2015; 7: 1124–1136.
  56. Pan MH, Chang YH, Badmaev V, Nagabhushanam K, Ho CT. Pterostilbene induces apoptosis and cell cycle arrest in human gastric carcinoma cell. *J Agric Food Chem.* 2007; 55: 7777–7785.
  57. Shamas-Din A, Kale J, Leber B, Andrews DW. Mechanisms of action of bcl-2 family proteins. *Cold Spring Harb Perspect Biol.* 2013; 5: a008714.
  58. Liao W, Luo Z, Liu D, Ning Z, Yang J, Ren J. Structure characterization of a novel polysaccharide from *Dictyophora indusiata* and its macrophage immunomodulatory activities. *J Agric Food Chem.* 2015; 63: 535–544.
  59. Liao W, Ning Z, Chen L, Wei Q, Yuan E, Yang J, Ren J. Intracellular antioxidant detoxifying effects of diosmetin on 2,2- azobis(2-amidinopropane) dihydrochloride (AAPH)-induced oxidative stress through inhibition of reactive oxygen species generation. *J Agric Food Chem.* 2014; 62: 8648–8654.
  60. Ermak G, Davies KJ. Calcium and oxidative stress: from cell signalling to cell death. *Mol Immunol.* 2002; 38: 713–721.
  61. Zheng S, Li X, Zhang Y, Xie Q, Wong YS, Zheng W, Chen T. PEG-nanolized ultra small selenium nanoparticles overcome drug resistance in hepatocellular carcinoma HepG2 cells through induction of mitochondria dysfunction. *Int J Nanomed.* 2012; 7: 3939–3949.

62. Liao WZ, Lu YJ, Fu JN, Ning ZX, Yang J, Ren JY. Preparation and characterization of dictyophora indusiata polysaccharide-zinc complex and its augmented antiproliferative activity on human cancer cells. *J Agric Food Chem*. 2015; 63: 6525–6534.
63. Hara K, Kasahara E, Takahashi N, Konishi M, Inoue J, Jikumaru M, Kubo S, Okamura H, Sato E, Inoue M. Mitochondria determine the efficacy of anticancer agents that interact with DNA but not the cytoskeleton. *J Pharmacol Exp Ther*. 2011; 337: 838–845.
64. Scherf U, Ross DT, Waltham M, Smith LH, Lee JK, Tanabe L, Kohn KW, Reinhold WC, Myers TG, Andrews DT, Scudiero DA, Eisen MB, Sausville EA, et al. A gene expression database for the molecular pharmacology of cancer. *Nat Genet*. 2000; 24: 236–244.
65. Musiani D, Hammond DE, Cirillo L, Enriquez J, Olivero M, Clague MJ, Flavia M, Renzo D. PIM2 kinase is induced by cisplatin in ovarian cancer cells and limits drug efficacy. *J Proteome Res*. 2014; 13: 4970–4982.
66. Chen ZF, Qin QP, Qin JL, Zhou J, Li YL, Li N, Liu YC, Liang H. Water-soluble ruthenium(II) complexes with chiral 4-(2,3-dihydroxypropyl)-formamide oxoaporphine(FOA): *in vitro* and *in vivo* anticancer activity by stabilization of G-Quadruplex DNA, inhibition of telomerase activity, and induction of tumor cell apoptosis. *J Med Chem*. 2015; 58: 4771–4789.
67. Song XF, Li LR, Shi Q, Lehmler HJ, Fu J, Su CY, Xia XM, Song E, Song Y. Polychlorinated biphenyl quinone metabolite promotes p53-dependent DNA damage checkpoint activation, S-phase cycle arrest and extrinsic apoptosis in human liver hepatocellular carcinoma Hep-G2 cells. *Res Toxicol*. 2015; 28: 2160–2169.
68. Wu CH, Wu DH, Liu X, Guoyiqibayi G, Guo DD, Lv G, Wang XM, Yan H, Jiang H, Lu ZH. Ligand-based neutral ruthenium(II) arene complex: selective anticancer action. *Inorg Chem*. 2009; 48: 2352–2354.
69. Wang CH, Shih WC, Chang HC, Kuo YY, Hung WC, Ong TG, Li WS. Preparation and characterization of amino-linked heterocyclic carbene palladium, gold, and silver complexes and their use as anticancer agents that act by triggering apoptotic cell death. *J Med Chem*. 2011; 54: 5245–5249.
70. Navarro JA, Salas JM, Romero MA, Vilaplana R, González-Viñchez F, Faure R. cis-[PtCl<sub>2</sub>(4,7-H-5-methyl-7-oxo [1, 2, 4]triazolo [1,5-a]pyrimidine)<sub>2</sub>]: a sterically restrictive new cisplatin analogue. Reaction kinetics with model nucleobases, DNA interaction studies, antitumor activity, and structure-activity relationships. *J Med Chem*. 1998; 41: 332–338.
71. Messori L, Orioli P, Tempand C, Marcon G, Biophys B. Interactions of selected gold(III) complexes with calf thymus DNA. *Res Commun*. 2001; 281: 352–360.
72. Kumar S, Xue L, Arya DP. Neomycin-neomycin dimer: An all-carbohydrate scaffold with high affinity for AT-rich DNA duplexes. *J Am Chem Soc*. 2011; 133: 7361–7375.
73. Jagadeesan S, Balasubramanian V, Baumann P, Neuburger M, Häussinger D, Palivan CG. Water-soluble Co(III) complexes of substituted phenanthrolines with cell selective anticancer activity. *Inorg Chem*. 2013; 52: 12535–12544.
74. Silva PP, Guerra W, Silveira JN, Ferreira-Ana MC, Bortolotto T, Fischer FL, Terenzi H, Neves A, Pereira-Maia EC. Two new ternary complexes of copper(II) with tetracycline or doxycycline and 1,10-phenanthroline and their potential as antitumoral: cytotoxicity and DNA cleavage. *Inorg Chem*. 2011; 50: 6414–6424.
75. Zhao JY, Ling X, Cao SS, Liu XJ, Wan SB, Jiang T, Li FZ. Antitumor activity of FL118, a survivin, Mcl-1, XIAP, and cIAP2 selective inhibitor, is highly dependent on its primary structure and steric configuration. *Mol Pharm*. 2014; 11: 457–467.
76. Cheng JJ, Khin KT, Davis ME. Antitumor activity of β-cyclodextrin polymer-camptothecin conjugates. *Mol Pharm*. 2004; 1: 183–193.
77. Sampson PB, Liu Y, Forrest B, Cumming G, Li SW, Edwards NK, Laufer R. The discovery of polo-like kinase 4 inhibitors: identification of (1R, 2S)-2-(3-((E)-4-(((cis)-2,6-dimethylmorpholino) methyl) styryl)-1 H-indazol-6-yl)-5'-methoxy Spiro [cyclopropane-1,3'-indolin]-2'-one (CFI-400945) as a potent, orally active antitumor agent. *J Med Chem*. 2014; 58: 147–169.
78. Evans IP, Spencer A, Wilkinson G. Dichlorotetrakis(dimethyl sulphoxide) ruthenium(II) and its use as a source material for some new ruthenium(II) complexes. *Dalton Trans*. 1973; 2: 204–209.